Pattern matching approach to pseudosymmetry problems in Electron Backscatter Diffraction

Gert Nolze[a], Aimo Winkelmann[b], Alan P. Boyle[c]

[a]*Dept 5.1, Federal Institute for Materials, Research and Testing (BAM), Unter den Eichen 87, 12205 Berlin, Germany*
[b]*Bruker Nano, Am Studio 2D, 12489 Berlin, Germany*
[c]*Dept of Earth, Ocean & Ecological Sciences, Herdman Building, 4 Brownlow Street, University of Liverpool, Liverpool L69 3GP, U.K.*

Abstract

We demonstrate an approach to overcome Kikuchi pattern misindexing problems caused by crystallographic pseudosymmetry in electron backscatter diffraction (EBSD) measurements. Based on the quantitative comparison of experimentally measured Kikuchi patterns with dynamical electron diffraction simulations, the algorithm identifies the best-fit orientation from a set of pseudosymmetric candidates. Using measurements on framboidal pyrite (FeS_2) as an example, we also show the improvement of the orientation precision using this approach.

Keywords: pyrite, EBSD, pseudosymmetry, cross-correlation, pattern simulation, Hough transformation, orientation precision

1. Introduction

The characterization of crystalline materials using electron backscatter diffraction (EBSD) in the scanning electron microscope (SEM) is a powerful tool for many different applications [1, 2]. However, a fundamental problem in EBSD analyses concerns possible misinterpretations (”misindexing”) of the measured Kikuchi patterns. Misindexing directly influences the qualitative detection of grains but also the quantitative characterization of grains and their boundaries. If misindexed data points are substituted in data-cleaning techniques, this can lead to questionable results [3]. Therefore, a correct orientation determination is a fundamental requirement for any subsequent microstructural characterization, and the prevention and the reliable correction of misindexing is clearly an important topic [4, 5].

Email address: Gert.Nolze@bam.de (Gert Nolze)

To a large extent, the symmetry of Kikuchi patterns is governed by the point group of a crystal. Crucial examples for misindexing problems are caused by phases that give rise to Kikuchi patterns with an apparently higher point group symmetry than is expected for the analyzed phase. This phenomenon is described by the term pseudosymmetry, which has been discussed in several EBSD-related publications [3, 6–9]. In the presence of pseudosymmetry, an unequivocal orientation determination depends on the ability of the applied data analysis method to detect the significant deviations from the apparently higher symmetry. In this context, physics-based Kikuchi pattern simulations [10] can be helpful to quantify the potential symmetry breaking parts of a Kikuchi pattern, the scope of which can limit our actual ability to detect the corresponding changes in the experimental data.

Using framboidal pyrite (FeS_2) as an example, we show in the present paper how misindexing of pseudosymmetric Kikuchi patterns can be corrected by a pattern matching approach [10, 11]. The comparison of experimentally measured Kikuchi patterns with dynamical electron diffraction simulations [12] makes it possible to identify the best-fit orientation from a set of pseudosymmetric candidates based on their cross-correlation coefficients. This procedure also quantifies the theoretical dissimilarity of the pseudosymmetric Kikuchi pattern candidates and thus allows estimation of the experimental limits of pseudosymmetric orientation discrimination. Additionally, the pattern matching approach also provides refined orientation parameters, which, in the investigation presented here, are at least two-times more precise than the values from the conventional orientation determination.

2. Experimental Details

2.1. Sample description

We investigate pseudosymmetry effects in framboidal pyrite from the Chattanooga Shale. Collection and sample preparation is given in detail in [7].

The pyrite framboids are typically 10 µm in diameter with individual microcrystals of pyrite being $<$ 1 µm in diameter, cf. Fig. 1 (a). Microcrystals within a given framboid vary little in size, and typically present idiomorphic crystals of cuboctahedral habit. The microcrystals may appear systematically arranged as shown in Fig. 1 (a) or disordered [7]. The framboids tend to occur in clusters within the sample and are associated with marcasite, an orthorhombic polymorph of FeS_2, and quartz.

2.2. Data acquisition

The orientation maps have been generated using a field-emission SEM LEO1530 VP (ZEISS) with a Bruker EBSD system. The acceleration voltage was 20 kV and the beam current was $\approx$ 7 nA. The collected

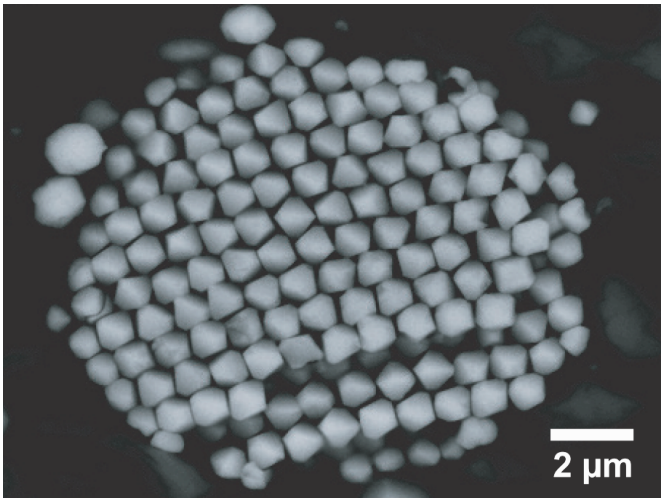

(a)

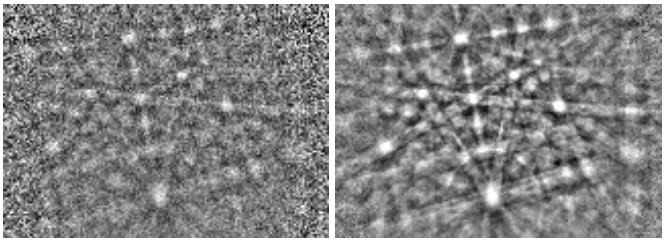

(b) **(c)**

Figure 1: A backscattered electron image of framboidal pyrite before EBSD preparation (a) shows a highly-ordered arrangement of individually grown cuboctahedral microcrystals of pyrite [7]. Despite the comparatively long acquisition time a single, the background-corrected experimental Kikuchi pattern (160× 120 pixels) in (b) is of low quality. The pattern in (c) represents the average of 32 single patterns collected in one microcrystal.

EBSD patterns were binned down on-chip to a size of 160×120 pixels. All collected raw Kikuchi patterns were stored in a data file for offline re-analysis and post-processing [13, 14]. An isometric grid at spacing 60 nm was chosen for the orientation maps of framboids.

The maximal possible dwell time per frame was 15 ms. In order to improve the signal-to-noise ratio, 3 camera frames have been averaged for each individual Kikuchi pattern, see Fig. 1 (b). For noise-reduced Kikuchi patterns derived from standard orientation maps, a pattern averaging algorithm has been applied [11]. This approach averages a number of Kikuchi patterns from a circular region of interest. The patterns are selected automatically on the basis that they show the best match to the reference pattern given by the central position of the selected region.

2.3. Data processing

EBSD data acquisition and indexing has been done using ESPRIT 1.94 (Bruker Nano). The Kikuchi pattern indexing was set up to work with between 12 and 6 identified Kikuchi bands. For the simulation of theoretical Kikuchi patterns, and for the discrimination between the pseudosymmetric orientations, we used ESPRIT *DynamicS*. The optimization of the orientational fit between the simulated and the experimental Kikuchi pattern in *ESPRIT DynamicS* involves reprojection of simulated test patterns from the theoretical master data, where the step size in orientation space is dynamically adapted according to the progress of the fit procedure. The removal of systematically misindexed data points by enforcement of consistent neighboring orientations (see below) was carried out in Tango (Channel5, Oxford Instr.).

All orientation and misorientation maps presented here have been created using the free and open-source Matlab toolbox MTEX [15]. MTEX offers inverse pole figure (IPF) color keys that suppress arbitrary color discontinuities for nearby orientations [16]. Moreover, MTEX colorizes EBSD orientation maps with respect to the, in general non-centrosymmetric, point-group of a phase instead of only the centrosymmetric Laue group [10, 17]. This also includes coloring according to the proper rotation (enantiomorphic) groups [18], which are relevant for a correct description of crystal orientations.

3. Theoretical Prerequisites

3.1. Pseudosymmetry

The symmetry of a crystal property or the phenomenon observed as result of a crystal property can be higher than the symmetry of the crystal itself and we thus may not be able to derive the full crystal symmetry from a measurement of the respective property (Neumann's principle) [19]. This can be due to *theoretically necessary* restrictions that the symmetry of the crystal structure places on a physical property tensor.

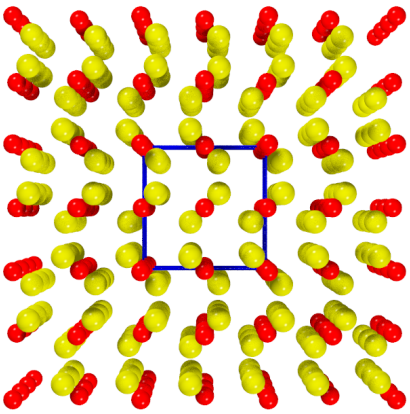

Figure 2: Crystal structure of pyrite projected along ⟨0 0 1⟩. Fe atoms are in red, S atoms in yellow. The square (black lines) indicates shape and dimension of the cubic unit cell and reflects an apparent four-fold rotation symmetry. However, the atomic distribution in projection only displays a two-fold rotation symmetry.

In this investigation, we use the term "pseudosymmetry" to describe an *experimental* limitation to detect deviations from a higher symmetry in a measured Kikuchi pattern (resulting from the interaction of electrons with the crystal structure). For instance, this can be caused by an inadequate analytical model for the interpretation of the experimental data [10], or by an insufficient signal-to-noise ratio. As the symmetry of Kikuchi patterns is governed to a large extent by the point group of a crystal, it is crucial to classify the patterns according to the presence and absence of characteristic symmetry elements. This can be experimentally challenging if the symmetry breaking is small and thus, effectively, a higher symmetry ("pseudosymmetry") is assigned to the pattern. The resulting equalization of nonequivalent crystal orientations is central to the misindexing problem in the presence of pseudosymmetry.

3.2. Symmetry of the pyrite crystal structure

As indicated by the extended Hermann-Mauguin symbol $P\ 2_1/a\ \bar{3}$, the crystal structure of pyrite does not contain any four-fold rotation or screw axis parallel to ⟨0 0 1⟩ [20]. The missing 90° rotation operation can be seen by the arrangement of the S-dumbbells within the structure shown in Fig. 2.

For pyrite, pseudosymmetry effects in Kikuchi patterns are caused by an experimentally relatively small symmetry breaking, which makes the differentiation between the actual point and Laue group $m\bar{3}$ of pyrite and the closely related, higher symmetric Laue group $m\bar{3}m$ difficult. Accordingly, Kikuchi bands representing {1 0 2} and {0 1 2} only seem to be equivalent, but for $m\bar{3}$ they are bands of independent lattice planes described by different intensities. The reason for this peculiarity is given by the crystal structure. As can be seen in Fig. 2, the Fe atom (red) positions are identical with the positions of the lattice points, i.e. their arrangement reflects the higher symmetry $m\bar{3}m$. In contrast, the arrangement of the S-dumbbells (yellow)

Table 1: Multiplicities of general and special face forms for all cubic crystal classes. The bold numbers display these forms which enable a differentiation to $m\bar{3}m$.
For $m\bar{3}$ beside the general form $\{h\,k\,l\}$ only $\{h\,k\,0\}$ fulfills this condition.

face form	23	$m\bar{3}$	432	$\bar{4}3m$	$m\bar{3}m$
{1 0 0}	6	6	6	6	6
{1 1 1}	**4**	8	8	**4**	8
{1 1 0}	12	12	12	12	12
$\{h\,k\,0\}$	**12**	**12**	24	24	24
$\{h\,h\,l\}$	**12**	24	24	**12**	24
$\{h\,k\,l\}$	**12**	**24**	**24**	**24**	48

shows a 180° rotation axis instead of a 90° rotational symmetry for the Fe substructure. This means that only the distribution of S is responsible for the reduction of the symmetry to a two-fold axis.

Moreover, the influence of the pseudosymmetry is specific to various $\{h\,k\,l\}$. This point group related effect can be discussed using the different multiplicities of lattice planes, cf. Table 1. If for two point groups the multiplicities of a plane $\{h\,k\,l\}$ are identical, these $\{h\,k\,l\}$ cannot be used for a symmetry-based differentiation between both point groups. This is closely related to the possibility of point group discrimination of a crystal based on its habit. For example, the existence of an octahedron as single form {1 1 1} excludes the point groups 23 and $\bar{4}3m$, but leaves the possibilities $m\bar{3}$, 432 and $m\bar{3}m$.

From Table 1 it follows that for any crystal with point group symmetry $m\bar{3}$ all Kikuchi bands representing {0 0 1}, {1 1 0}, {1 1 1} and $\{h\,h\,l\}$ will reflect an apparently four-fold rotational symmetry, whereas – except for the general plane $\{h\,k\,l\}$ – only planes of the type $\{h\,k\,0\}$ will enable differentiation between $m\bar{3}$ and $m\bar{3}m$. This is a significant restriction because {0 0 1}, {1 1 0}, {1 1 1} and $\{h\,h\,l\}$ are often represented by strong Kikuchi bands. Because only a limited number of bands are used for interpretation, as high as 12 but as low as 6 in this study, there is a potentially decreasing probability of detecting a sufficient number of the critical $\{h\,k\,0\}$ or $\{h\,k\,l\}$.

3.3. Pseudosymmetry in Kikuchi patterns of pyrite

3.3.1. General features

Although the symmetry-breaking in the pyrite structure is clearly visible in Fig. 2, a prediction about the visible impact on the Kikuchi patterns is not straightforward. In order to get a qualitative impression about the difference between two pseudosymmetric orientation solutions, theoretical simulations of the experimental Kikuchi pattern in Fig. 1(b+c) before and after 90° rotation around $\langle 0\,0\,1\rangle$ are shown in Fig. 3(a) and (b).

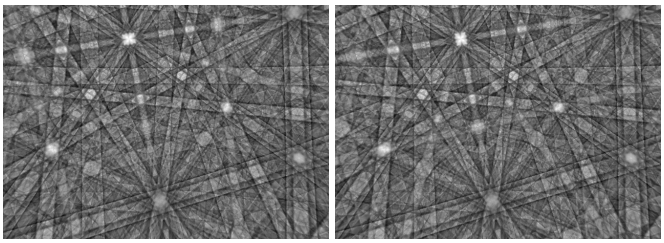

(a) correct solution: r =0.626 **(b)** incorrect solution: r =0.525

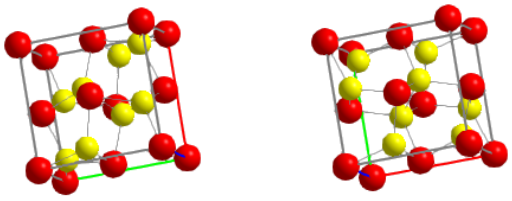

(c) **(d)**

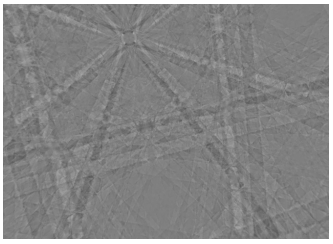

(e) difference: (a)-(b)

Figure 3: (a,b): Simulation of pseudosymmetric solutions of the experimental pattern given in Fig. 1, with (b) rotated by 90° around ⟨0 0 1⟩ relative to (a). r is the cross-correlation coefficient between the simulation and the experimental pattern in Fig. 1. (c,d): crystal orientations of (a,b). (e): The weak intensity difference between (a) and (b) mainly displays the non-equivalent bands of {1 0 2} and {0 1 2}, and the broader bands of {2 0 3} and {0 2 3}.

At first glance, the two simulated intensity distributions in Fig. 3(a) and (b) look very similar. However, the difference signal image in (e) makes the differences between the two pseudosymmetric patterns directly visible.

Inspecting the difference signal in more detail, and remembering the discussion about the lattice planes {0 0 1}, {0 1 1}, {1 1 1} and {h h l} in Section 3.2, it is not surprising that these Kikuchi bands do not contribute to the difference signal at all. The crucial signal for a differentiation of the pseudo-symmetric solutions is only formed by Kikuchi bands coming from general {h k l}, and from special {h k 0}. Unfortunately, these planes form weak diffraction intensities in the Kikuchi pattern. An unequivocal differentiation between pseudosymmetric solutions for pyrite will be impossible as long as this predictable behavior is not considered within the indexing algorithms applied.

3.3.2. Element-resolved Analysis

Because of the different positions of the Fe and S atoms within the unit cell, it follows that these atoms will produce different element-specific diffraction patterns, which can give a deeper insight into the origin of the pseudosymmetry problem. The corresponding parts of the total intensity backscattered by Fe and S, respectively, can be discussed by using dynamical simulations to separate these respective contributions.

As seen in Fig. 3(c) and (d), a difference between both pseudosymmetric solutions is already suggested by the atomic configuration. Whereas the Fe-atoms (green) occupy identical positions in both displayed orientations, the S-atoms (red) are differently distributed. Fig. 4 summarizes how the element-related diffraction signal is affected by these orientation-specific atomic configurations.

In order to quantify the differences between the pseudosymmetric orientations, we use an element-specific normalized difference $A_S(x)$ for x =Fe, S_2, FeS_2 which is calculated as

$$A_S(x) = \frac{I(x,0) - I(x,90)}{I(FeS_2,0) + I(FeS_2,90)}. \quad (1)$$

Because of its lower atomic number and the Z^2-dependence of the Rutherford scattering cross section, a single S atom ($Z = 16$) is backscattering less electrons than an Fe atom ($Z = 26$). However, the integrated S signal is still in a sizeable order of 75% of the Fe signal since there are twice as many S as there are Fe-atoms in pyrite. Because of the face-centered distribution of Fe, the resulting diffraction signal is very close to showing a 90° rotational symmetry, as can be seen Fig. 4(a). The small deviations between both pseudo-symmetrically related Fe patterns in Fig. 4(b) have their origin in the fact that the Kikuchi signal emitted from the high-symmetry distributed Fe is still influenced by the entire FeS_2-structure, i.e. also by the lower symmetry of the S-distribution. The weak difference signal, which is responsible for the deviation of the Fe pattern from the four-fold symmetry, is thus mainly delivered by the S-atoms (Wyckhoff position 8c: x,x,x; x=0.385). The individual contribution of the backscattering from S atoms to the overall signal is shown in (c), whereas the normalized difference for the S contribution is displayed in (d). Both clearly exhibit the symmetry $m\bar{3}$ of pyrite. A comparison between the total normalized difference in Fig. 4(f) and (d) shows that the total signal in (e) is rather dominated by Fe (a), but the total difference signal in (f) mainly shows the contribution of the S (d) atoms.

4. Experimental Results

4.1. Peculiarities in Orientation Maps of Pyrite

An automated orientation mapping experiment was carried out to test the practical effects of pseudosymmetry in pyrite Kikuchi patterns, see Fig. 5. The results of indexing using conventional band detection by

Hough transformation of the background-processed Kikuchi patterns gave inconsistent solutions for a number of microcrystals in the pyrite framboid studied. This is seen by a systematic color speckling in the pyrite microcrystals in Fig. 5(a), which was confirmed as misindexing due to pseudosymmetry by investigating the misorientation between differently colored adjacent pixels within pyrite microcrystals.

It is well-known that the probability of a correct orientation solution in any EBSD analysis is affected by the pattern quality, which affects the grade of band detection. Pattern quality also varies with crystal orientation [21], meaning differently oriented grains might be more or less prone to misindexing. Kikuchi patterns collected on framboidal pyrite are of noticeably low quality.

However, pyrite misindexing also occurs in samples which produce much better quality Kikuchi patterns (e.g. [22] where up to 5% of analyzed points were affected by pseudosymmetry issues). Therefore, the pattern quality by itself is not the dominant cause of pseudosymmetric misindexing.

Unfortunately, for some point group symmetries speckled grains can be produced simply by improper color keys. It has been shown in [16] that, for seven of eleven centrosymmetric Laue groups, the standard key used in commercial software packages can generate color jumps within grains. In order to prevent any such color discontinuities, we used the MTEX [15] color key shown in Fig. 5(d). The application of this color key is meaningful for two reasons. First, the color key is optimized to prevent any color jumps within grains, which are in effect regions of practically the same orientation. Second, it describes the fundamental sector of the enantiomorphic symmetry group 23 instead of the commonly applied Laue group $m\bar{3}$. Whereas the key for 23 can differentiate between mirror-symmetric but non-equivalent crystal orientations, the key for $m\bar{3}$ can only indicate a symmetry-equivalent crystallographic description of a single reference direction.

4.2. Correction of Pseudosymmetric Solutions

4.2.1. The Use of Higher Symmetry

For phases like martensite or γ-TiAl, which are tetragonal but pseudo-cubic, it is well-accepted practice to substitute the real crystal symmetry with the higher-symmetric enantiomorphic point or centrosymmetric Laue group because the two pseudosymmetric solutions cannot be distinguished experimentally. The relative atomic positions are identical in the correct as well as in the pseudosymmetric unit cell, and the crystal lattice is only slightly distorted, so the Kikuchi bands show practically the same intensities and their positions are only insignificantly shifted so these examples are usually considered to be hopeless cases. Similar conditions also exist if lattice parameters are practically multiplied in order to consider a systematic ordering of elements, e.g. zincblende and chalcopyrite [23].

Another case is given by phases like pyrite in which the crystal lattice reflects a higher symmetry but the atomic positions can only be described in a lower symmetry class. Some EBSD software enables a manipulation of the Laue group, e.g. to prevent the visualization of inaccurate indexing. This is of course only acceptable in exceptional cases. For the case of pyrite a pretense of a higher symmetry class is neither necessary nor recommended.

4.2.2. Orientation Enforcement

A possible method to suppress the misindexed data points seen in Fig. 5(a) is to force the misindexed points into a consistent orientation with respect to their neighboring points during a post-processing procedure. To this end, a transformation operator Ω describing the relationship between the pseudosymmetric orientations needs to be defined. Ω is preferably given as rotation by an angle ϕ around a specific lattice vector $[u\,v\,w]$ and a maximum tolerable deviation angle $\Delta\phi$. For pyrite it is described be a 90° rotation around $\langle 0\,0\,1\rangle$.

The orientation enforcement can be described as follows: two orientations g_i and g_j of adjacent measurement positions will only be made consistent with each other if they do not already belong to the same grain. This means that prior to this post processing procedure, a grain detection is required. If the application of Ω ends up in a relationship

$$(g_j \cdot \Omega) \approx g_i, \tag{2}$$

the initial orientation g_j will be replaced by the consistently enforced orientation $(g_j \cdot \Omega)$. The result of this procedure applied on the data set displayed in Fig. 5(a) is shown in Fig. 5(b). The color speckling within grains has disappeared, and each grain is now characterized by consistent nearby orientations of the same color shade. Mathematically, for the specific example of pyrite, this means that the third Euler angle φ_2 will be replaced by $(\varphi_2 + 90°)$ if (2) is true. The two other Euler angles φ_1 and ϕ are kept unchanged. In this approach no smoothing or averaging of surrounding orientation data is applied.

However, this relatively simple and obviously effective procedure has a major weakness. The reference orientation g_i is assumed to be the correct one, which might not be the case. In practical consequence, a grain orientation can be switched completely into the wrong orientation. In Fig. 5(b) at least the grains encircled in red have been rotated into the minor orientation shown in Fig. 5(a). From this it follows that the selection of g_i as the true orientation is necessarily correct even if the majority orientation in a grain is used as g_i.

The orientation enforcement method is risky for additional reasons. If adjacent grains happen to have

a misorientation that falls within the parameters set for the relationship in (2), then one of the grains will be rotated to be consistent with the other. This has occurred for at least one grain in Fig.5(b); circled in green and marked by an arrow. In unprocessed Fig. 5(a) this joint grain is differentiated as two grains, dove-colored and emerald green. This effect will become systematic if the described pseudosymmetry is simultaneously also a twin law, as is possible e.g. for quartz with Dauphinée twins. Then the twin-related bands are not always correctly recognized so that the twin-symmetric orientation also appears as pseudosymmetric solution so that an orientation enforcement will erase all twins in a microstructure.

Thus, it is clear that the orientation enforcement method can produce serious artifacts that not only affect the orientation distribution, but will also influence the characterization of grain and phase boundaries.

4.2.3. Pattern Matching

An alternative way to correct the pseudosymmetric orientation data is a pattern-matching approach, which in the case of pseudosymmetry compares the experimental Kikuchi pattern with simulations of all possible pseudosymmetric solutions. One major advantage in comparison to the conventional Hough-related indexing is that the pattern matching method automatically takes all characteristic features into account. A fundamental requirement for this approach is a realistic intensity simulation of the pattern. The matching will decide unequivocally which of the pseudosymmetric solution is correct and result in a map that shows definitely correct solutions. Fig. 6(a) summarizes in yellow the orientations incorrectly indexed by Hough-related indexing. Misindexing occurs practically in every grain, but more so in some grain orientations than others.

In order to increase the indexing efficiency (hit rate) even more, a suitable $m\bar{3}m$ phase can be used for indexing as discussed in section 4.2.1. Using austenite, because it corresponds to the Fe positions of pyrite which are the major contributors of the Kikuchi signal (section 3.3.2), pushes the hit rate from 72% in Fig. 5(a) and (b) to 86% in (c). As already indicated in section 4.2.1, the resulting orientations determined by the Hough-related indexing and using the higher symmetry should be statistically half wrong, which is confirmed by Fig.6(b) comparing the blue (correct) and yellow (pseudosymmetric) colored pixels. On the other hand, the number of correct and pseudosymmetric solutions is higher, and – in contrast to indexing with pyrite – the resulting grains have uniform orientation. The correction of all yellow-marked orientations in Fig. 6(b) using the pattern-matching approach results in the orientation distribution in Fig. 5(c).

Fig. 5 (c) shows the distinction between the orientation description by orientation enforcement (section 4.2.2 and Fig. 5 (b)) and the pattern matching approach using either the same orientation data (hit rate:

72%, not shown) or a re-indexing with a perhaps better matching phase (hit rate: 86%, Fig. 5 (c)). The resulting ≈ 8% grains identified as misinterpreted by orientation enforcement are highlighted in red circles in Fig. 5 (c). While this outcome is specific to this investigation of framboidal pyrite microstructure it raises the more general issue of EBSD accuracy, which will depend on the pseudosymmetry character of the respective phase, the pattern quality, and the orientation distribution.

4.2.4. Precision Enhancement

In addition to providing a quantitative criterion for deciding between pseudosymmetric orientations using the cross-correlation coefficient r, the pattern-matching approach can also be slightly adapted to increase orientation precision considerably. Thus, there is general application of this approach beyond purely resolving pseudosymmetry issues, i.e. the orientation refinement approach can be used for improved orientation mapping where no pseudosymmetry effects occur.

For the framboidal pyrite discussed here, the impact of orientation refinement is clearly visible in Fig. 5(c) where the colors of several grains after pattern-matching reflect less color-variations compared to (b). However, assuming a starting point of well-orientated, homogeneous crystals (see Fig. 1(a)), the difference in orientation precision can be much better visualized by comparing Kernel average misorientation (KAM) maps for both post-processing methods, cf. Fig. 7. KAM is commonly used to visualize the local orientation variation around a selected pixel. The accumulated and averaged misorientation to the surrounding measurement positions display local orientation gradients. KAM can be also applied as a way of visualizing "orientation noise", i.e. how precisely crystal orientations can be determined using locally collected Kikuchi patterns.

Despite the fact that the Kikuchi patterns collected on framboidal pyrite are far from ideal quality for determination of misorientations, cf. in Fig. 7b, the KAM maps impressively demonstrate the advantage of the pattern-matching related orientation refinement method (c) compared to a Hough-related orientation determination (a). The orientation refinement approach delivers clearly less orientation variations within grains. Only towards the boundaries does lower orientation precision arise; this result can be explained by poor Kikuchi pattern quality at pyrite microcrystal edges or by the effect of superimposing Kikuchi patterns from adjacent microcrystals. However, whereas the cross-correlation coefficient map (d) shows a clear correlation to the KAM map in (c), the PQ map in (b) does not reflect a convincing correlation to the grains displayed in the Hough-related KAM map in (a). This is an indication that the Hough-related orientation precision is more affected by the actual crystal orientation than by the pattern matching approach.

It is also possible to evaluate orientation precision in EBSD maps by investigating the correlated misorientation angle, which is defined as the frequency distribution of misorientation angles calculated between a definable number of randomly selected pairs of orientation measurements. The term "correlated" indicates that the second position has to be closer than typically 3 pixels to the first position. The resulting histograms are displayed in Fig. 8. Despite the small grains and the potential impact of microcrystal edge and superimposing Kikuchi patterns, the graphs demonstrate that the precision of the refinement using a pattern-matching approach is at least two times better than orientation determination using conventional peak detection in Hough space.

In this respect, data-processing using pattern-matching is a tool for refinement of orientation information delivered from the conventional Hough-transform based methods. It can reduce and evaluate misindexing, but by refinement it can also increase the angular precision for more sophisticated analysis of EBSD data.

5. Conclusions and Summary

In this paper, we have discussed several key issues related to relevant pseudosymmetry problems occurring in electron backscatter diffraction measurements. This leads to the following conclusions for the prevention of unreliable results during real-time and/or post-processing of orientation data:

- Pseudosymmetric orientation solutions need to be corrected properly because a correct orientation determination is fundamental for any subsequent microstructural characterization.
- A simple enforcement of consistent orientations based on the detection of pseudosymmetric neighboring misorientations will lead to artifacts in orientation maps and pole figures. The amount of misinterpretations depends on the phase-specific extent of the pseudosymmetry, but also on experimental factors which affect the required detection of symmetry sensitive features within the patterns.
- Incorrect grain orientations also affect the grain boundary characterization. Only the misorientation within grains (e.g. GAM and KAM) will be not affected since the absolute orientation of the grain is irrelevant.
- A pattern matching approach comparing experimental and dynamically simulated Kikuchi patterns can be used to differentiate between pseudosymmetric solutions for each individual measurement point.

- A quantification of the pseudosymmetric pattern similarity (here using the cross-correlation coefficient) also helps to estimate the limits of the possible orientation discrimination in specific phases.

- The cross-correlation based orientation refinement uses the Hough-related orientation description as starting data. Compared to the Hough-related orientations, the refined data lead to an improved orientation precision which is at least two times higher for the framboidal pyrite analyzed in this study.

It should be obvious from the above that to take advantage of the pattern-matching approach, all collected Kikuchi patterns must be saved for post-processing.

Acknowledgement

We thank Michaela Buchheim (BAM) for sample preparations and light-microscopical support, and Romeo Saliwan Neumann (BAM) for the EBSD data acquisition. Dr. Ralf Hielscher (TU Chemnitz) is acknowledged for his continuous support regarding the efficient application of MTEX, including the integration of all point-group-sensitive color keys. The sample was provided by Hiroaki Ohfuji.

References

[1] A. J. Schwartz, M. Kumar, B. L. Adams (Eds.), Electron Backscatter Diffraction in Materials Science, 1st Edition, Kluver Academic/Plenum Publishers, New York, Boston, Dordrech, London, Moscow, Netherlands, 2000.

[2] A. J. Schwartz, M. Kumar, B. L. Adams, D. P. Field (Eds.), Electron Backscatter Diffraction in Materials Science, Springer Science+Business Media, 2009.

[3] L. Brewer, J. Michael, Risks of "cleaning" electron backscatter diffraction data, Microscopy Today 3 (2010) 10–15.

[4] D. J. Prior, E. Mariani, J. Wheeler, Electron Backscatter Diffraction in Materials Science, Springer Science + Business Media, 2009, Ch. 12. EBSD in the Earth Sciences: Applications, Common Practice, and Challenges, pp. 345–360.

[5] T. Karthikeyan, M. K. Dash, S. Saroja, M. Vijayalakshmi, Evaluation of misindexing of EBSD patterns in a ferritic steel, J. Microsc. 249 (1) (2013) 26–35.

[6] D. J. Prior, A. P. Boyle, F. Brenker, M. C. Cheadle, A. Day, G. Lopez, L. Peruzzo, G. J. Potts, S. Reddy, R. Spiess, N. E. Timms, P. Trimby, J. Wheeler, L. Zetterström, The application of electron backscatter diffraction and orientation contrast imaging in the SEM to textural problems in rocks, Amer. Mineral. 84 (1999) 1741–1759.

[7] H. Ohfuji, A. P. Boyle, D. J. Prior, D. Rickard, Structure of framboidal pyrite: An electron backscatter diffraction study, Amer. Mineral. 90 (2005) 1693–1704.

[8] C. Zambaldi, S. Zaefferer, S. I. Wright, Characterization of order domains in $\gamma-$TiAl by orientation microscopy based on electron backscatter diffraction, J. Appl. Cryst. 42 (6) (2009) 1092–1101.

[9] R. C. Hildyard, S. Llana-Fnez, J. Wheeler, D. R. Faulkner, D. J. Prior, Electron backscatter diffraction (EBSD) analysis of bassanite transformation textures and crystal structure produced from experimentally deformed and dehydrated gypsum, J. Petrology 52 (5) (2011) 839–856.

[10] A. Winkelmann, G. Nolze, Point-group sensitive orientation mapping of non-centrosymmetric crystals, Appl. Phys. Lett. 106 (2015) 072101.

[11] A. Winkelmann, G. Nolze, Chirality determination of quartz crystals using electron backscatter diffraction, Ultramicroscopy 149 (2) (2015) 58–63.

[12] A. Winkelmann, C. Trager-Cowan, F. Sweeney, A. P. Day, P. Parbrook, Many-beam dynamical simulation of electron backscatter diffraction patterns, Ultramicroscopy 107 (4-5) (2007) 414–421.

[13] R. A. Schwarzer, J. Hjelen, Orientation microscopy with fast EBSD, Mater. Sci. Technol. 26 (6) (2010) 646–649.

[14] E. Payton, G. Nolze, The backscatter electron signal as an additional tool for phase segmentation in electron backscatter diffraction, Microsc. Microanal. 19 (4) (2013) 929–941.
[15] F. Bachmann, R. Hielscher, H. Schaeben, Texture analysis with MTEX–free and open source software toolbox, Sol. State Phenom. 160 (2010) 63–68.
[16] G. Nolze, Discontinuities in inverse pole figure (IPF) colouring, EBSD Conference of the Royal Microscopy Society (RMS), Oxford (2013).
[17] R. Hielscher, G. Nolze, Orientation color maps in MTEX, ICOTOM 17, Dresden (2014).
[18] G. Nolze, Euler angles and crystal symmetry, Cryst. Res. Technol. 50 (2) (2015) 188–201.
[19] J. Nye, Physical Properties of Crystals: Their Representation by Tensors and Matrices, Oxford University Press, Oxford, 1985.
[20] T. Hahn (Ed.), International Tables for Crystallography. Volume A: Space-group symmetry, 4th Edition, Kluver Academic Publishers, Dordrecht/Boston/London, 1995.
[21] S. R. Claves, A. Deal, Orientation dependence of EBSD pattern quality, Microsc. Microanal. 11 (2005) 514–515.
[22] C. D. Barrie, A. P. Boyle, D. J. Prior, An analysis of the microstructures developed in experimentally deformed polycrystalline pyrite and minor sulphide phases using electron backscatter diffraction, J. Struct. Geology 29 (2007) 1494–1511.
[23] D. Abou-Ras, J. Gibmeier, G. Nolze, A. Gholinia, P. Konijnenberg, On the capability of revealing the pseudosymmetry of the chalcopyrite-type crystal structure, Cryst. Res. Technol. 43 (3) (2008) 234–239.

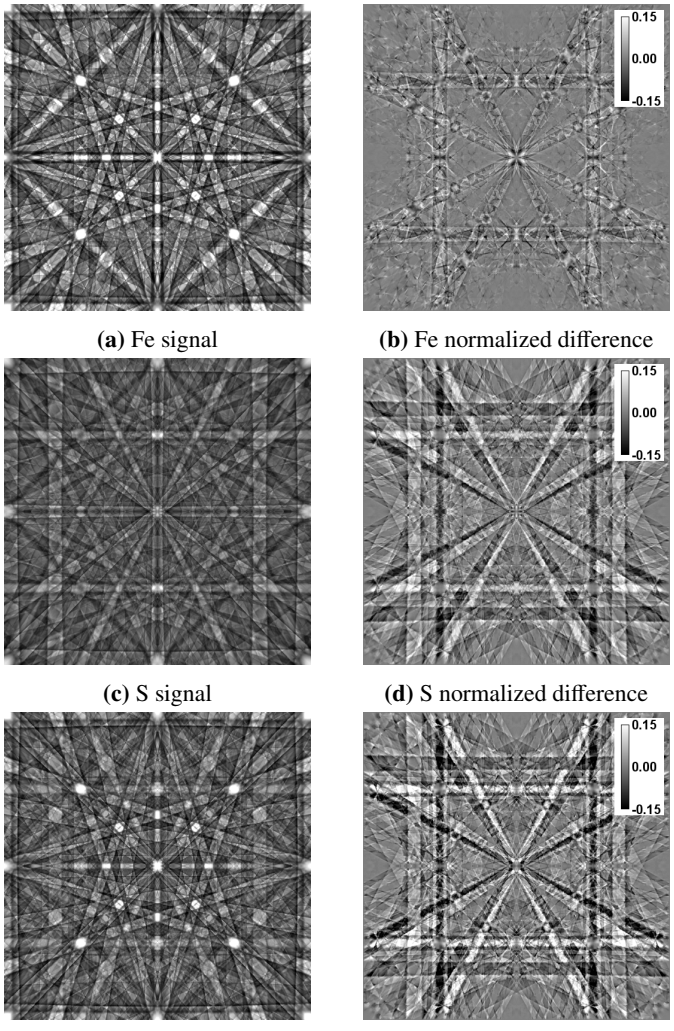

(a) Fe signal **(b)** Fe normalized difference

(c) S signal **(d)** S normalized difference

(e) FeS_2 signal **(f)** FeS_2 normalized difference

Figure 4: Element-resolved Kikuchi patterns in pyrite, gnomonic projection centered at ⟨0 0 1⟩ which is also the pattern center. The corners define ⟨1 1 1⟩, and the midpoints indicate ⟨0 1 1⟩.
Contribution of each element – Fe (a) and S (c) – to the overall signal of pyrite (e)=(a)+(b). The respectively normalized differences A_S between pseudosymmetric orientations are given in (b), (d) and (f).

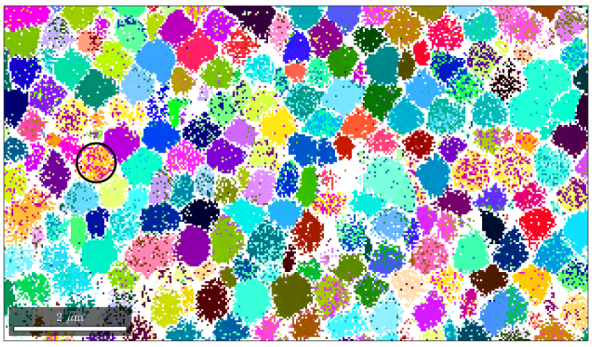

(a) as indexed (72%)

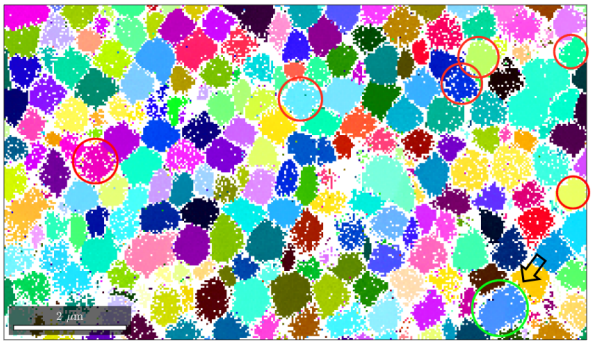

(b) consistent orientation enforcement

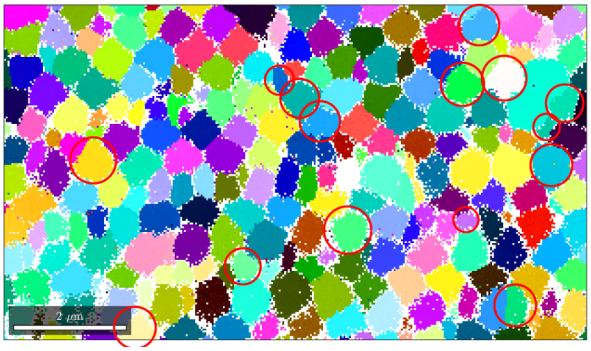

(c) re-indexed (86%, $m\bar{3}m$) + pattern matching

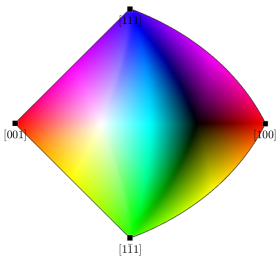

(d) IPF color key

Figure 5: IPF-maps of framboidal pyrite after different post-processing steps. Non-colored positions (white) are locations of unsolved Kikuchi patterns. (a) displays the initial orientation data (at least 6 of 12 bands indexed). (b) represents the same data as (a) but with a consistently enforced orientation solutions as described in 4.2.2. (c) is based on the same data-set but indexed with a generic face-centered cubic phase (austenite) and subsequently a cross correlation. (d) displays the color key for the proper rotation group 23. See text for explanation of the circles.

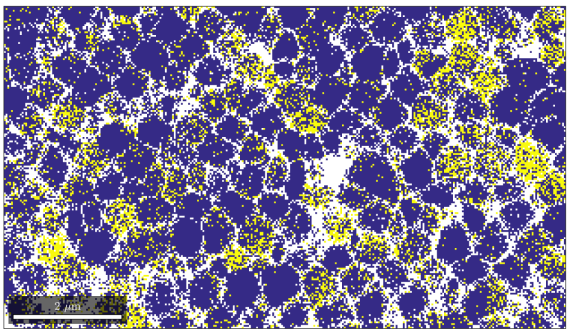

(a) Orientation switching applied to $m\bar{3}$-indexed patterns (Fig. 5a)

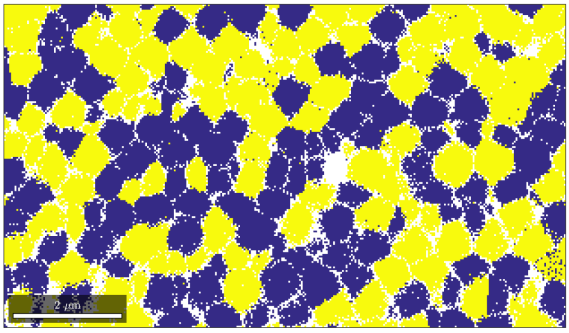

(b) Orientation refinement from $m\bar{3}m$-indexed patterns to $m\bar{3}$

Figure 6: Evaluation of Hough-related indexing by pattern matching. Blue pixels reflect correct orientation, yellow pixels display pseudosymmetric orientation, whereas white pixels mark positions where either no indexing was possible, or the cross-correlation coefficient r between experiment and pattern simulation was $r < 0.08$.
(a) 16% of the solved patterns were incorrectly assigned by Hough-related indexing, cf. Fig. 5(a).
(b) Using austenite ($m\bar{3}m$) as phase, nearly 20% more patterns could be uniformly indexed, but the half of all solved patterns was described by their pseudosymmetric orientations and needed to be corrected using the matching procedure.

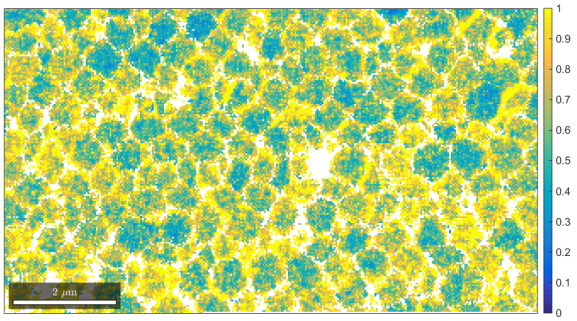

(a) KAM, Hough-related indexing

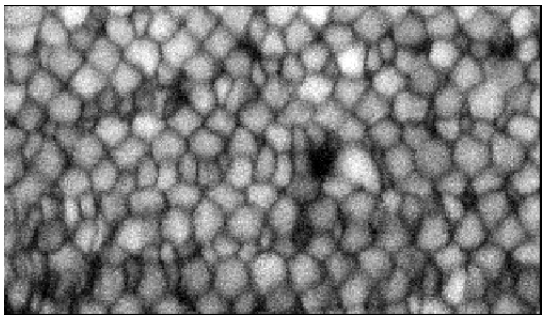

(b) pattern quality map

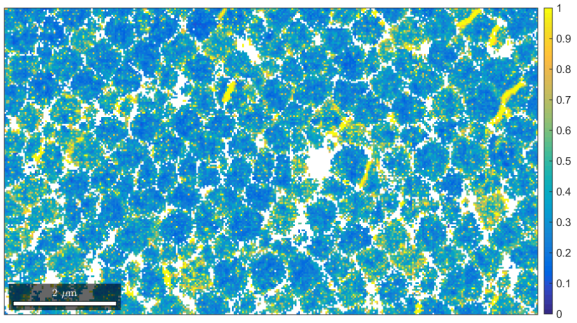

(c) KAM, refinement by pattern matching

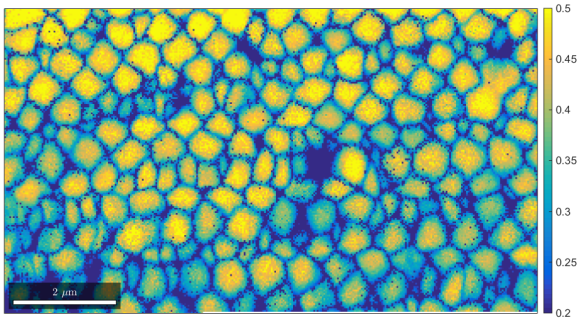

(d) cross-correlation coefficient *r*

Figure 7: (a) Kernel average misorientation (KAM) and (b) pattern quality maps derived from the Hough-related orientation solutions. The KAM map (c) of the same measurement after orientation refinement using the pattern-matching approach shows less orientation variations within grains than the conventional result in (a). The map of the cross-correlation coefficient of the measured Kikuchi patterns with respect to the best fit simulation is shown in (d).

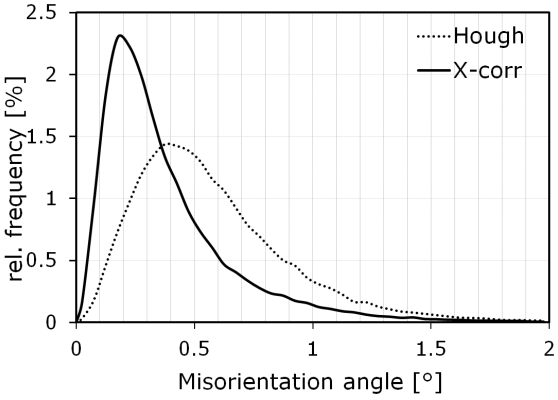

(a) misorientation distribution

Figure 8: The correlated misorientation distribution (Channel5, Oxford Instr.) in indicates a twice higher precision for the pattern matching – X-corr, Fig. 7(b) – in comparison to the Hough-related standard orientation determination (a). The class width applied was 0.05°.